Loughborough
University

This item was submitted to Loughborough's Institutional Repository (https://dspace.lboro.ac.uk/) by the author and is made available under the following Creative Commons Licence conditions.

For the full text of this licence, please go to:
http://creativecommons.org/licenses/by-nc-nd/2.5/

Plastic Behaviour of Microstructural Constituents of Cortical Bone Tissue: A Nanoindentation Study

Adel Abdel-Wahab, Vadim V. Silberschmidt

Wolfson School of Mechanical and Manufacturing Engineering, Loughborough University, Loughborough, Leicestershire, LE11 3TU, UK

E-mail: a.a.abdel-wahab@lboro.ac.uk

E-mail: v.silberschmidt@lboro.ac.uk

Abstract

A mechanical behaviour of bone tissues is defined by mechanical properties of its microstructural constituents. Also, those properties are important as an input for finite-element models of cortical bone to simulate its deformation and fracture behaviours at the microstructural level. The aim of this study was to investigate a post-yield behaviour of osteonal cortical bone's microstructural constituents at different loading rates, maximum load levels and dwell times; nanoindentation with a spherical-diamond-tip indenter was employed to determine it. The nanoindentation results revealed significant difference in stiffness values of cortical bone's microstructural features − interstitial matrix and osteons. Similarly, interstitial matrix exhibited a stiffer post-yield behaviour compared to that of osteons that reflects the relationship between the post-yield behaviour and collagen maturity. In addition, both osteons and interstitial matrix demonstrated a time-dependent behaviour. However, in order to assess elastic-plastic behaviour accurately, an effect of viscosity on nanoindentation results was reduced by using a time-delay method.

Keywords: cortical bone; nanoindentation; flow stress; flow strain; osteons; interstitial matrix; post-yield.

1.   Introduction

Bone is a natural composite material with hierarchical organization at different length scales. At the nano-scale, it consists of a collagen matrix impregnated with ceramic nano-particles known as *carbonated hydroxyapatite* (Currey 1999; Fratzl *et al*. 2004). At the micro-scale, cortical bone is in the form of lamellar layers of 5 µm thickness. Similar to a plywood structure, inside a layer, collagen fibres are parallel; however, their orientations are different for different layers. Across a bone section, not all lamellae are arranged in the same way; for instance, near the outer and inner surfaces, lamellae are parallel and arranged along the cortical bone's circumference. On the other hand, the outside and inside circumferential lamellae form a region made of circular structures called *osteons*, formed from concentric lamellae within remnants of a bone's remodelling process called *interstitial matrix*. The interface between osteons and interstitial matrix is called *cement line*; it is a collagen-free and highly mineralized layer. Cement lines have an important effect on bone's behaviour, especially its fracture. Osteons are, on average, 200 µm in diameter and 1 cm long and parallel to the bone's longitudinal axis (Ethier and Simmons 2007). In addition, a network of canals and channels is formed across the bone's section and along its axis; these canals accommodate blood vessels and called *Haversian canals*. Moreover, bone has living cells (osteocytes) that live within an interconnected network of microscopic channels known as *canaliculi*. The latter are responsible for exchange of nutrients and waste between osteocytes [3]. At the millimetre length scale, bone consists of a dense and thick outer layer called

cortical bone and a sponge-like structure known as *trabecular bone* (Peterlik *et al.* 2006). All these hierarchical levels work together to enhance macroscopic mechanical properties of bone tissue at the full-bone scale (Peterlik *et al.* 2006).

Characterisation of mechanical properties of cortical bone's microstructural constituents is essential not only for understanding a mechanical behaviour of the entire bone tissue, but also for developing adequate finite-element models to simulate its fracture, deformation and cutting (Alam *et al.* 2010). Thanks to micro- and nano-indentation techniques, it is possible to measure mechanical properties in a region as small as $1\,\mu$m (Cowin 2001). Depth-sensing nanoindentation together with theoretical methods can be used for extracting an elastic modulus from load-displacement data (Doerner and Nix 1986; Oliver and Pharr 1992). Over the last two decades, the nanoindentation technique has achieved very high resolution for both loads and displacements as well as a submicron spatial resolution, e.g., load resolution of 0.3 μN and displacement resolution of 0.16 nm (Doerner and Nix 1986; Oliver and Pharr 1992). With this technique, mechanical properties of microstructural features of interest can be derived from the analysis of high-resolution load-displacement data obtained as the indenter is driven into, and withdrawn from, the specimen leaving a residual imprint on its surface (Oliver and Pharr 1992), see Fig. 1. For instance, the elastic modulus of those features can be determined from the slope of the unloading portion of the measured load-displacement curve, whereas their hardness can be calculated from the measured peak load and the residual indentation area, see Appendix for theoretical basis of nanoindentation method. A hardness measurement conveys data about the quality and degree of bone mineralization (Cowin 2001). General mechanical property characterisation of cortical bone at its microstructural level is essential for development of finite-element numerical models capable not only to capture its mechanical behaviour, but also to predict its fracture at that scale. Nanoindentation has been shown to be a suitable tool for quantifying the material properties of bone's microstructural constituents, such as osteons and trabeculae (Rho *et al.* 1997; Lewis, and Nyman 2008). Since many of the cortical bone tissue's features of interest are at the micro-scale level, nanoindentation technique is capable of directly probing its intrinsic mechanical properties at that level. Other methods were also used to measure bone's microscopic properties: microhardenss, microtesting, *in-vivo* microindentation and ultrasonic techniques (Weaver 1966; Rho 1993; Ko *et al.* 1995; Shieh *et al.* 1995; Diez-Perez *et al.* 2010).

Recently, an increased number of studies were performed to measure the elastic modulus and hardness of cortical bone using different indenters and at different anatomical positions (Turner *et al.* 1999; Rho *et al.* 2002; Hengsberger *et al.* 2003, Hoffler *et al.* 2000). For instance, Hoffler *et al.* (2005) investigated the effect of different nanoindentation's experimental parameters on the results of measurements of the microstructural mechanical properties of a human cortical bone tissue. The studied parameters included the specimen preparation conditions, indentation depth, repetitive loading, time delay, and displacement rate. It was concluded that consistent values of the elastic modulus can be obtained from a 500 nm-deep indent. Also, it was found that the modulus and hardness values of dry specimens were significantly higher than those of wet specimens – by 22.6% and 56.9%, respectively. In addition, there were differences in the modulus values obtained at different loading rates: values at 5 nm/s were smaller than those obtained at 10 nm/s and 20 nm/s while there was no significant difference in data obtained at those higher rates. In another study, Rho *et al.* (1997) used a combination of atomic force microscopy (AFM) and nanoindentation to measure the elastic modulus and hardness values of human cortical bone and trabecular bone tissues. The aim of that study was to analyse the advantage of the AFM-mode compared to conventional microscopy. It was found that the former was a very useful tool for surface characterization and precise selection of indentation area. The measured elastic moduli

ranged from 18$\pm$1.7 GPa for a single bone structural unit (BSU) of human cortical bone to 22.5$\pm$3.1 GPa for BSU of trabecular bone. The obtained hardness levels were in the range between 0.6$\pm$0.11 GPa for cortical bone and 1.1$\pm$0.17 GPa for trabecular bone (Hengsberger *et al.* 2001). For human tibia bone, elastic moduli measured with nanoindentation were 22.5$\pm$1.3 GPa for the osteons and 25.8$\pm$0.7 GPa for the interstitial lamellae. Different studies revealed a significant difference between the mechanical properties of osteons and interstitial matrix (Rho *et al.* 1997; Zysset *et al.* 1999). Those differences could be due to several factors, such as degree of mineralization, collagen fibre orientation, and arrangement of those materials (Rho et al. 1997; Zysset *et al.* 1999; He and Swain 2007). More recently, the inelastic response of the cortical bone tissue studied using the nanoindentation technique was reported (Carnelli *et al.* 2010). Although the literature data demonstrate that mechanical properties of microstructural features of bones such as elastic modulus and hardness were captured by various teams, yet complete constitutive equations, i.e., stress-strain curves at that scale length level are still not available. From all the mechanical properties of cortical bone's microstructural constituents, their stress-strain behaviour is one of the most important because it provides us with their deformation response. Based on that behaviour, phenomena, such as plasticity localization, crack initiation and propagation as well as crack interaction with cortical bone's microstructural features can be assessed, using advanced modelling techniques. In this paper, in addition to measuring the elastic modulus and hardness values of cortical bone constituents, the flow stress-flow strain relationships for osteons and interstitial matrix are measured – to the author's knowledge – for the first time using a spherical indenter tip at different loading rates, maximum load levels and dwell times.

2.   Materials and Methods
2.1.   Preparation of Specimens

Four specimens were cut from a fresh bovine femur bone (aged 1.5-2 years), collected from a local butcher. The flesh was removed and the bone was chilled before collection. The mid-part of the femur (diaphysis) was extracted using a band-saw at a speed of 40 m/min. Then, the diaphysis part of the femur was cleaned again to ensure that the outer layer of the cortical bone reached and there was no remaining fat or flesh. The specimens were cut from the posterior anatomical position using a low-speed diamond saw with water cooling. Specimens with dimensions $(5 \times 3 \times 15)$ mm^3 were used in a nanoindentation experiment. The nanoindentation specimens were ground using a series of grinding papers Standard ANSI grit- 240, 600, 1200- and then polished with cloth of 1 μm grits so that the morphology of the osteonal cortical bone could be observed with the nanoindentation's optical microscope (see Fig. 2). Specimens were stored at room temperature in 0.9% saline solution until tested.

2.2.   Experimental Method

The nanoindentation tests were performed with the Nano-test 600 indentation system (Micro Materials ltd., Wrexham, UK) at room temperature (23.3°C) and ambient humidity level of 31.7%. A spherical diamond tip with a radius of 25 μm with a low-load head for 0.1-500 mN was employed, and a maximum measurement depth when the system is set at full sensitivity is approx. 1.5 μm. A NanoTest (NT2) material testing platform (Fig. 3) was used to calibrate, and set control parameters; it also allowed monitoring and analysing the experimental data. The specimen - the transverse-radial posterior section of the mid-diaphysis of bovine cortical bone - was glued horizontally to a holder and gently firmed in front of the indenter tip. The microscope accompanying the indenter tip allowed precise positioning of the indenter at the required position to test either the osteons or the interstitial matrix, see Fig. 3.

Nanoindentation tests were performed for four identical cortical bone specimens cut from the posterior cortex position in the transverse-radial plane at maximum loads of 5 mN, 10 mN, 20 mN and 50 mN, with each specimen being tested under one loading condition. The specimen tested under a maximum load of 10 mN was also employed to investigate the effect of loading rate on the elastic-plastic behaviour with three different rates of 0.5 mN/s, 1 mN/s and 2 mN/s; the rest of the specimens were tested at loading rate of 0.5 mN/s. For each specimen, two indents with 100 µm separating distance were performed within three osteons and for three interstitial matrix positions. For each indent, ten loading-unloading cycles were performed to construct the flow stress-flow strain curve, with each cycle constituting a point on the curve. Apart from the final unloading cycle, the minimum load achieved in unloading was 50% of the maximum load of the respective cycle. For all loading conditions and rates, to investigate the effect of holding time, each indent was performed twice with dwell times of 0 s and 120 s. The tests were performed in a load-control regime with recording both the indentation load and displacement.

A view of the experimental arrangement of the bovine cortical bone's indentation test is shown in Fig. 4.

3.   Results

Recently, the nanoindentation technique has been applied to biological tissues including a bone tissue (Zysset *et al*. 1999). Measuring the mechanical properties of cortical bone at the lamellar level is important for developing theoretical micromechanical models and finite-element schemes along with gaining better understanding of bone's fracture mechanisms. Since many of the features of interest in cortical bone are at microscopic level, its intrinsic mechanical properties at that level can be probed directly by nanoindentation technique. A load-displacement curve for nanoindentation test shows that as the load increases, the indenter sinks in the material causing elastic-plastic deformation. On the other hand, when unloading the indenter, the material recovers mainly elastically. Using this technique, the elastic modulus, post-yield behaviour and hardness of cortical bone tissue were characterized as discussed below.

3.1.   Elastic Modulus and Hardness

The nanoindenter with a spherical tip with radius of 25 µm made imprints on the bone specimens' surface, clearly visible under a light microscope (see Fig. 5). The shape of indents is nearly spherical, demonstrating that a nanoindenter could easily make small indents within desired microstructural features of cortical bone tissues such as osteons and interstitial bone. No cracks were found around the spherical imprints.

The basic response acquired with the depth-indentation system is a load-displacement curve representing the loading-unloading history of the sample. The typical cyclic load-displacement (depth) curves for osteons and interstitial matrix obtained in the indentation tests at maximum load of 20 mN, loading-unloading rate of 0.5 mN/s and two time delays −0 s and 120 s − are shown in Fig. 6. The used load-control method showed a different indentation depth for osteons and interstitial matrix at the same indentation load. For instance, a maximum load of 20 mN corresponded to depths of 823.3 nm and 1194 nm for osteons at the last cycle, while they were 602.5 nm and 1038 nm at the same load in the interstitial matrix for time delays of 0 s and 120 s, respectively. It was the case for all the performed cycles indicating that stiffness of interstitial matrix exceeded that of osteons. Moreover, for the time delay of 120 s, both osteons and interstitial matrix demonstrated higher depths when

compared to those acquired at the time delay of 0 s indicating a viscoelastic nature of the cortical bone tissue.

Using both the experimental data acquired and the theoretical method described in Appendix, mechanical properties such as elastic modulus and hardness can be obtained using Eq. 12 and Eq. 11, respectively (see Appendix). Calculations of the elastic modulus were based on the unloading part of the load-displacement curve. Also, a Poisson's ratio of 0.42 was used for the microstructural feature of cortical bone tissue. Figure 7a shows the effect of loading-unloading rate on the elastic modulus values of osteons and interstitial matrix measured with different time delays – 0 s and 120 s. Generally, the values of elastic modulus were higher for interstitial matrix compared to osteons for all the loading-unloading rates, 0.5 mN/s, 1 mN/s and 2 mN/s, and for the time delays, 0 s and 120 s. For the time delay 0 s, the moduli measured for osteons were 12.9$\pm$1.08 GPa, 13.05$\pm$0.81 GPa and 13.48$\pm$1.1 GPa while those for interstitial matrix were 14.29$\pm$1.72 GPa, 14.30$\pm$1.65 GPa and 14.90$\pm$1.5 GPa for loading-unloading rates of 0.5 mN/s, 1 mN/s and 2 mN/s, respectively. On the other hand, for time delay of 120 s, the moduli measured were 7.68$\pm$0.53 GPa, 8.89$\pm$1.06 GPa and 11.90$\pm$1.03 GPa for osteons and 9.5$\pm$0.05 GPa, 9.63$\pm$0.77 GPa and 13.22$\pm$1.71 GPa for interstitial matrix for loading-unloading rates of 0.5 mN/s, 1 mN/s and 2 mN/s, respectively. Based on these results, it can be noticed that for time delay of 0 s, significant difference between elastic moduli was found neither for osteons nor for interstitial matrix at the studied loading rates. For the time delay of 120 s, there were no significant differences between the values of elastic modulus for loading rates of 0.5 mN/s and 1 mN/s, whereas a significant difference was found between values measured at these rates and 2 mN/s for both osteons and interstitial matrix. For the maximum−indentation−load study (see Fig. 7b), the elastic moduli for interstitial matrix were higher than those of osteons at the same indentation load for both time delays. For the time delay of 0 s, the elastic moduli increased with the maximum-load increase for loads of 5 mN and 10 mN, while the values were approximately the same for loads of 20 mN and 50 mN (both for osteons and interstitial matrix).

The average hardness values were 0.39$\pm$0.008 GPa, 0.42$\pm$0.019 GPa, 0.435$\pm$0.03 GPa and 0.518$\pm$0.064 GPa for osteons and 0.618$\pm$0.012 GPa, 0.622$\pm$0.015 GPa, 0.634$\pm$0.094 GPa and 0.765$\pm$0.048 GPa for interstitial bone tissue for maximum loads of 5 mN, 10 mN, 20 mN and 50 mN, respectively. As expected, these values were slightly lower than those obtained in literature using a sharp indenter tip due to the larger area accompanied with the spherical tip that led to lower hardness values. In the literature, hardness values of 0.578$\pm$0.052 GPa for osteons and 0.818$\pm$ 0.049 GPa for interstitial matrix were reported, obtained for bovine cortical bone at a maximum load of 20 mN using Berkovich indenter (Thurner 2009). However, in order to quantify the elastic-plastic behaviour of cortical bone tissue at microstructural scale, a spherical tip had to be used to obtain a smooth transition from the elastic behaviour to plastic one.

3.2. Flow Stress and Flow Strain

Ten-cycle indentation tests were performed for both the osteonal area and interstitial matrix, with flow stresses and strains calculated for each cycle using the obtained experimental data together with Eqs. 13 and 14, see Appendix. As an example, the calculated flow stress-flow strain curves for osteons and interstitial matrix at loading-unloading rate of 0.5 mN/s and time delay of 120 s are demonstrated in Fig. 8. Since the nanoindentation technique leads to elastic-plastic deformation, using cyclic loading with spherical indenter enabled us to resolve elastic and plastic responses. Accordingly, each point on these curves is the result of one complete cycle of loading-unloading indentation test. Then, the quadratic regression was used

with high correlation factors to fit the experimental data for both constituents (Fig. 8). It was found that not only the elastic modulus and hardness values of the interstitial matrix were higher than those of osteons, but also the flow stresses required to achieve the same flow strains were higher.

By investigating the loading-unloading effect on the post-yield behaviour, it was found that cortical bone's microstructural features (osteons and interstitial matrix) are strain-rate sensitive as apparent from comparison of the respective flow stress–flow strain curves for different loading rates (Fig. 9). The higher the loading rate, the higher the values of flow stresses at the same flow strains. These results indicate that cortical bone at the microstructural level possesses strain-rate-sensitive elastic-plastic behaviour demonstrated by the effect of loading rate on the elastic modulus values as shown in Fig. 7 and on the plastic response as shown in Fig. 9. The flow stress-flow strain graphs are higher for higher strain rates. Moreover, the response indicates a hardening effect for both osteons and interstitial matrix. However, the interstitial matrix shows nearly perfectly-plastic behaviour for a loading rate of 1 mN/s. It is worth noticing also that for higher strain rates, the material started to yield at lower flow strain for both osteons and matrix. Indents in all the series gave the same behaviour with some slight changes in the values of the flow stresses and strains. Most probably, the changes in those values were due to local variations in properties linked to collagen maturity, surface porosity, subsurface lacunae, or irregularities that remain after polishing (Hoffler *et al.* 2005).

4. Discussion

In this study, nanoindentation tests with a spherical indenter were performed to study mechanical behaviour of microstructural constituents of cortical bone tissue - osteons and interstitial matrix - in order to quantify their elastic properties, hardness and post-yield behaviour. The fact that bone is in a continuous remodelling process consisting in a succession of resorption and formation processes that lead to heterogeneity of bone material, and the correlation between the mineral content and elastic modulus underpin the difference between elastic properties of the osteon and interstitial matrix (Hoc *et al.* 2006; Bala *et al.* 2011). Additionally, the results of this study showed lower levels of variation of the elastic modulus for osteons compared to those for interstitial matrix for all loading rates. Again, the variance in the elastic modulus values was likely related to mineral, collagen and non-collagenous protein composition (Hoffler *et al.* 2005). Moreover, there may have been other sources of variance including subsurface porosity, subsurface lacunae, and surface irregularities (Hoffler *et al.* 2005). Though, only a slight difference was found between the elastic-modulus values for time delays 0 s and 120 s for a maximum load of 50 mN. It can be noticed here that as the indentation load increases as, in turn, the indentation depth, the values of elastic modulus converge. This can be linked to the surface polishing artifact and inaccurate area estimation for shallow indents. The depth-sensitivity findings are in line with a similar study by (Hoffler *et al.* 2005). The average elastic properties obtained in our experiment were comparable to data in the literature, elastic moduli in the range from 2 to 45.8 GPa were reported for different animal species including bovine bone (Abdel-Wahab *et al.* 2010, Thurner 2009), and in the range from 13.4 GPa to 24.2 GPa for bovine bone osteons (Hoc *et al.* 2006). However, the obtained elastic-modulus data were sometimes lower compared to some of those available in the literature because they have used sharper indentation tip, such as Berkovich or a cube corner. In the current study, spherical indentation tip was used to obtain the elastic-plastic behaviour of cortical bone constituents that yielded higher indentation area, which, in turn, led to lower values of elastic moduli and hardness.

Obviously, it is well documented in literature that a bone mineral content plays a major role in bone strength, and a collagen component plays a role in plastic deformation (Currey 2003). In addition, in another study, it was shown that collagen maturity is a strong predictor of a cortical bone's plastic behaviour at microstructural level (Bala *et al.* 2011). In fact, the interstitial matrix is the remaining part of the remodelling process; hence, its age is higher than that of osteons. In this sense, its collagen component is more mature and consequently exhibits higher post-yield behaviour as indicated in Fig. 8. It is also important to note considerable deformability of both constituents. Moreover, when using nanoindentation to measure mechanical properties of the cortical bone tissue, significant effects on the results due viscoelasticity may arise, since the method of Oliver and Pharr (1992), assumes a purely elastic behaviour during unloading. One method to reduce the error due to viscosity effects in the Oliver-Pharr analysis is increasing the time delay before unloading (Rho and Pharr 1999). Hence, the effect of the time delay was considered for the post-yield behaviour as shown in Fig. 10. A significant difference was found between the flow stress-flow strain behaviours obtained based on a time delay of 0 s and 120 s for both osteons and interstitial matrix. Obviously, the use of the higher time delay produced higher values of flow strain due to the creep effect but required lower levels of flow stress. Also, the harder material − interstitial matrix − exhibited a more pronounced change in the gradient of flow stress as flow strain increased. Both constituents showed a gradual work hardening under the indenter as the load is increased in every subsequent cycle. This means that plastic deformation started to occur beneath the indenter surface but it was constrained by the surrounding elastic material at the beginning, then the plastic region extended to the surface of the specimen and continued to grow. It was suggested in another study that most of the bone's toughness takes place after yielding, in which energy depends on both strength and ductility, i.e., a degree of permanent deformation of bone (Nyman *et al.* 2007). Obviously, two different constituents exhibited different behaviours; the interstitial matrix demonstrated higher post-yield toughness – measured as the area under the flow stress-flow strain curve – than osteons; this was the case for different loading rates. The constituents showed a quadratic hardening, with magnitudes and slopes for osteons being different than those for the interstitial matrix. Because of the hierarchical organizations of a cortical bone tissue, it is believed that different toughening mechanisms at the microstructural level could be responsible for higher toughness of interstitial matrix. It suggested that global viscoelasticty of cortical bone is defined by viscoelastic properties of its constituents at the microstructural level. The next stage of our research will be devoted to quantification of this link.

5.   Conclusions

In this study, the mechanical behaviour of microstructural constituents of cortical bone tissue - osteons and interstitial matrix – were studied using nanoindentation technique in order to quantify their elastic properties, hardness and post-yield behaviour. The nanoindentation results demonstrated higher stiffness values for interstitial matrix compared to those of the osteons. This difference is related to the heterogeneity of cortical bone due to continuous remodelling processes that result in gradients in the mineral content. Also, cortical bone's microstructural constituents (osteons and interstitial matrix) exhibited elastic-visco-plastic behaviour with a stiffer post-yield behaviour of interstitial matrix compared to that of osteons. This behaviour reflects the relationship between the post-yield behaviour and collagen maturity. Moreover, the viscous effect on the nanoindentation results was reduced by using the time-delay method. Now, the obtained elastic-plastic behaviour of cortical bone tissue's microstructural constituents can be implemented in finite-element models to study microstructural processes of deformation and fracture.

References

Abdel-Wahab, A.A., Alam, K., and Silberschmidt, V.V. (2011) 'Analysis of anisotropic viscoelastoplastic properties of cortical bone tissues' Journal of Mechanical Behaviour of Biomedical Materials, Vol. 4 No. 5, pp. 807-820.

Alam, K., Mitrofanov, A.V. and Silberschmidt, V.V. (2010) 'Thermal analysis of orthogonal cutting of cortical bone using finite element simulations', International Journal of Experimental and Computational Biomechanics, Vol. 1, No. 3, pp.236–251.

Bala, Y., Depalle, B., Douillard, T., Meille, S., Clément, P., Follet, H., Chevalier, J., and Boivin, G. (2011) 'Respective roles of organic and mineral components of human cortical bone matrix in micromechanical behavior: an instrumented indentation study' Journal of Mechanical Behaviour of Biomedical Materials, Vol. 4 No 7, pp. 1473-1482.

Carnelli, D., Gastaldi, D., Sassi, V., Contro, R., Ortiz, C., and Vena, P. (2010) 'A finite element model for direction-dependent mechanical response to nanoindentation of cortical bone allowing for anisotropic post-yield behavior of the tissue' Journal of Biomechanical Engineering, Vol. 132/ 081008-1– 081008-10.

Cowin, S.C. (2001) Bone Mechanics Handbook, 2nd ed., CRC Press LLC, Florida, USA

Currey, J.D. (1999) 'The design of mineralised hard tissues for their mechanical functions' Journal of Experimental Biology, Vol. 202, pp. 3285-3294.

Currey, J.D. (2003) 'Role of collagen and other organics in the mechanical properties of bone' Osteoporosis International, Vol. 14 Suppl. 5, pp. 29-36.

Diez-Perez, A., Güerri, R., Nogues, X., Cáceres, E., Peña, M. J. , Mellibovsky, L., Randall, C., Bridges, D., Weaver, J. C., Proctor, A., Brimer, D., Koester, K. J., Ritchie, R. O., and Hansma, P. K. (2010) 'Microindentation for in vivo measurement of bone tissue mechanical properties in humans' Journal of Bone and Mineral Research, Vol. 25, No. 8, pp. 1877–1885.

Doerner, M.F., and Nix, W.D. (1986) 'A method for interpreting the data from depth-sensing indentation instrument' Journal of Materials Research, Vol. 1 No, 4, pp. 601-609.

Ethier, C.R., and Simmons, C.A. (2007) Introductory Biomechanics: From Cells to Organisms, Cambridge University Press.

Fratzl, P., Gupta H.S., Paschalis, E.P., and Roschger, P. (2004) 'Structure and mechanical quality of the collagen–mineral nano-composite in bone', Journal of Materials Chemistry, Vol. 14, pp. 2115-2123.

He, L.H., and Swain, M.V. (2007) 'Nanoindentation derived stress-strain properties of dental materials' Dental Materials, Vol. 23 No. 7, pp. 814-821.

Hengsberger, S., Enstroem, J., Peyrin, F., and Zysset, P.H. (2003) 'How is the indentation modulus of bone tissue related to its macroscopic elastic response? a validation study' Journal of Biomechanics, Vol. 36 No. 10, pp. 1503-1509.

Hengsberger, S., Kulik, A., and Zysset, P.H. (2001) 'A combined atomic force microscopy and nanoindentation technique to investigate the elastic properties of bone structural units' European Cells and Materials, Vol. 1, pp. 12-17.

Hoc, T., Henry, L., Verdier, M., Aubry, D., Sedel, L., and Meunier, A. (2006) 'Effect of microstructure on the mechanical properties of Haversian cortical bone' Bone, Vol. 38 No. 4, pp. 466-474.

Hoffler, C.E., Moore, K.E., Kozloff, K., Zysset, P.K., Brown, M.B., and Goldstein, S.A., (2000) 'Heterogeneity of bone lamellar-level elastic moduli' Bone, Vol. 26, No. 6, pp. 603–609.

Hoffler, C.E., Philippe, X.E.G., Zysset, K., and Goldstein, S.A. (2005) 'An applications of nanoindentation technique to measure bone tissue lamellae properties' Journal of Biomedical Engineering, Vol. 127 No. 7, pp. 1046-1053.

Ko, C.C., Douglas, W.H., and Cheng, Y.S. (1995) 'Intrinsic mechanical competence of cortical and trabecular bone measured by nanoindentation and micro-indentation probes' ASME Bioengineering Conference. San Francisco. AMSE-BED-Vol. 29, pp. 415-416.

Micro Materials Ltd (2004) NanoTest On-line Help File Version 1.0 and NanoTest Manual Version 3.0, Unit 3, the Byre, Wrexham Technology Park, UK.

Lewis, G., and Nyman, J. S., (2008) 'The use of nanoindentation for characterizing the properties of mineralized hard tissues: state-of-the art review' Journal of Biomedical Materials Research Part B: Applied Biomaterials, Vol. 87B, pp. 286–301.

Nyman, J.S., Roy, A., Tyler, J.H., Acuna, R.L., Gayle, H.J., and Wang, X. (2007) 'Age-related factors affecting the postyield energy dissipation of human cortical bone' Journal of Orthopaedic Research, Vol. 25 No. 5, pp. 646-655.

Oliver, W.C., and Pharr, G.M. (1992) 'An improved technique for determining hardness and elastic modulus using load and displacement sensing indentation experiment' Journal of Materials Research, Vol. 7 No. 6, pp. 1564-1583.

Peterlik, H., Roschger, P., Klaushofer, K., and Fratzl, P. (2006) 'Orientation dependent fracture toughness of lamellar bone' International Journal of Fracture, Vol. 139, pp. 395-405.

Rho, J.Y. (1993) 'Young's modulus of trabecular and cortical bone material: ultrasonic and microtensile measurements' Journal of Biomechanics, Vol. 26 No. 2, pp. 111-119.

Rho, J.Y., and Pharr, G.M. (1999) 'Effects of drying on the mechanical properties of bovine femur measured by nanoindentation' Journal of Materials Science: Materials in Medicine, Vol. 10 No. 8, pp. 485-488.

Rho, J.Y., Tsui, Y.T., and Pharr, G.M. (1997) 'Elastic properties of human cortical and trabecular lamellar bone measured by nanoindentation' Biomaterials, Vol. 18 No. 20, pp. 1325-1330.

Rho, J.Y., Zioupos, P., Currey, J.D., and Pharr, G.M. (2002) 'Microstructural elasticity and regional heterogeneity in human femoral bone of various ages examined by nano-indentation' Journal of Biomechanics, Vol. 35 No. 2, pp. 189-198.

Shieh, S.-J., Govind, S., Gudipaty, K., Subramanian, R., and Grimm, M.J. (1995) 'High resolution ultrasonic measurements of the material properties of cortical and trabecular bone in the human vertebrae' Bioengineering conference, R.M. Hochmuth, Langrana, N.A., and Hefzy, M.S. Beaver Creck, Colorado. ASME-BED-29, pp. 413-414.

Sneddon, I.N. (1965) 'The Relation between load and penetration in the axisymmetric Boussinesq problem for a punch of arbitrary profile' International Journal of Engineering Science, Vol. 3 No. 1, pp. 47-57.

Thurner, P.J. (2009) 'Atomic force microscopy and indentation force measurement of bone.' Wiley Interdisciplinary Reviews: Nanomedicine and Nanobiotechnology, Vol. 1 No. 6, pp. 624-649.

Turner, C.H., Rho, J.Y., Takano, Y., Tsui, T.Y., and Pharr, G.M. (1999) 'The elastic properties of trabecular and cortical bone tissues are similar: results from two microscopic measurement techniques' Journal of Biomechanics, Vol. 32, No. 4, pp. 437-441.

Weaver, J.K. (1966) 'The microscopic hardness of bone' The Journal of Bone & Joint Surgery, Vol. 48 No. 2, pp. 273-288.

Zihiqiang, C., and Zhang, X. (2008) 'Nanoindentation stress-strain curves of plasma-enhanced chemical vapor deposited silicon oxide thin films' Thin Solid Films, Vol. 516 No. 8, pp. 1941-1951.

Zysset, P.K., Guo, X.E., and Hoffler, C.E. (1999) 'Elastic modulus and hardness of cortical and trabecular bone lamellae measured by nanoindentation in the human femur' Journal of Biomechanics, Vol. 32 No. 10, pp. 1005-1012.
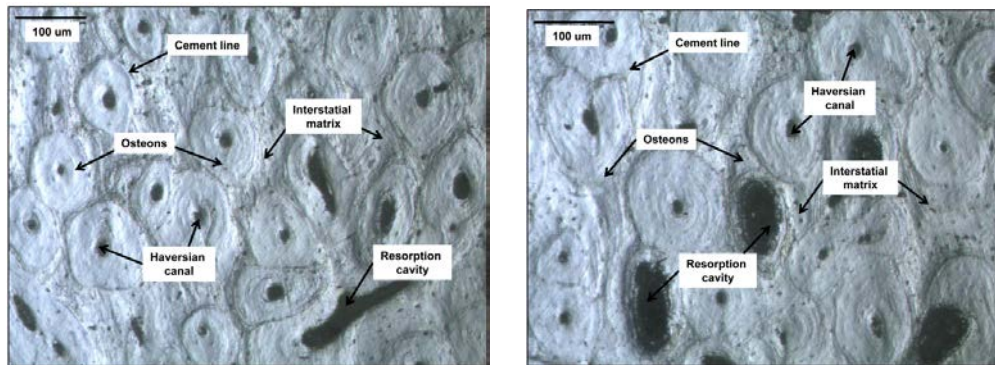
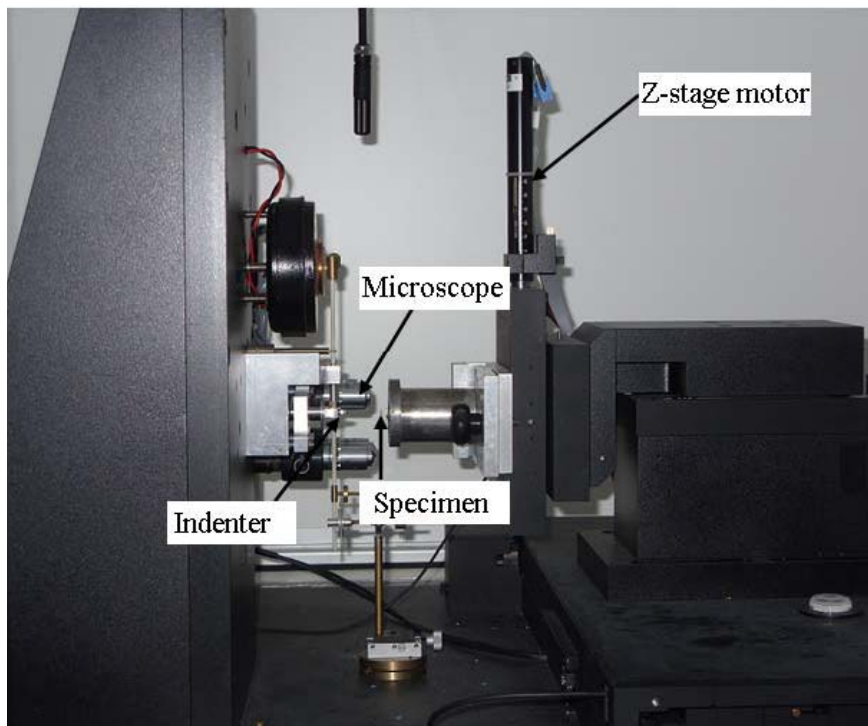Figure 1: Different optical-microscopy images of bovine femoral cortical bone tissue (posterior cortex)

Figure 2: Nano-Test 600 indentation system
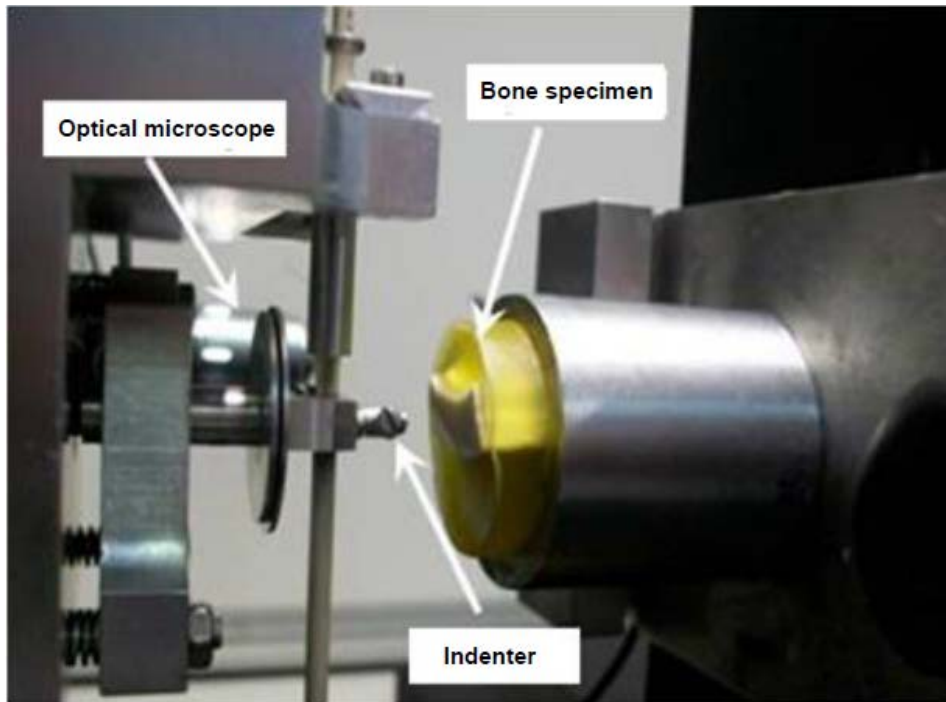
Figure 3: Experimental arrangements for nanoindentation test of bovine femoral cortical bone tissue
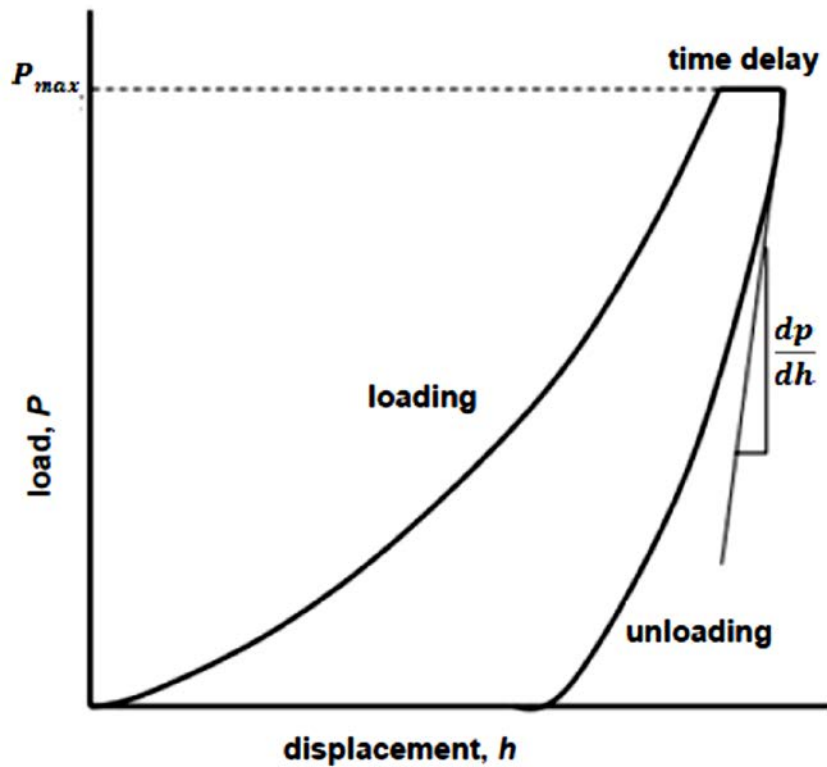
Figure 4: Schematic illustration of nanoindentation load-displacement curve during loading, time delay and unloading (after Oliver and Pharr (1992))
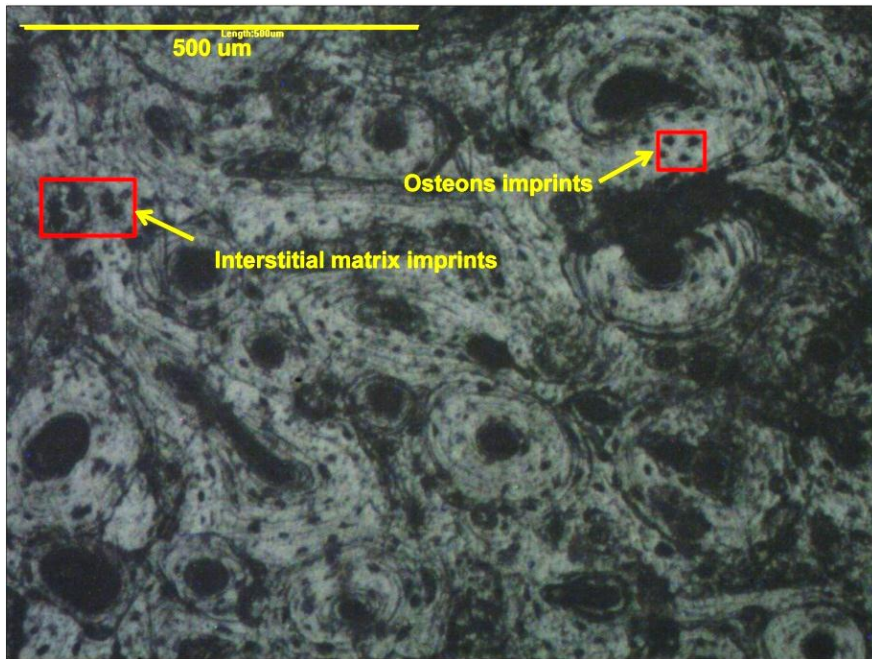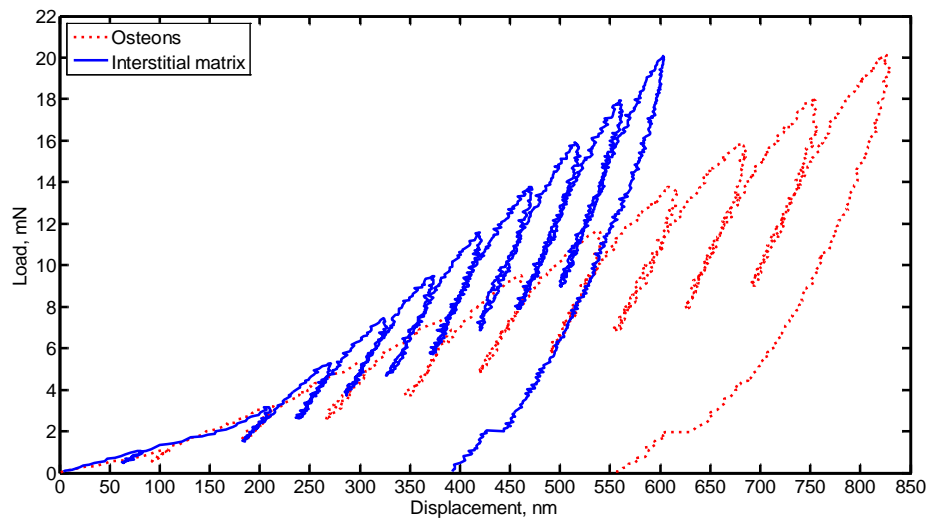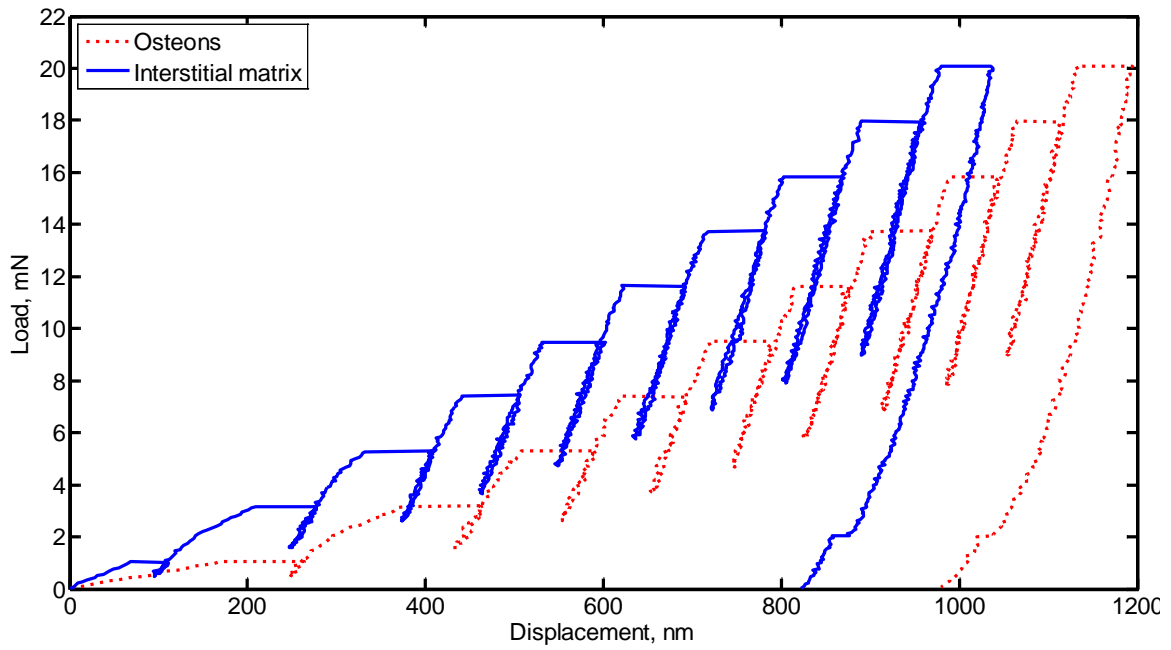
Figure 5: Spherical indents in osteons and interstitial matrix of cortical bone's specimen

(a)

(b)

Figure 6: Typical cyclic load-displacement curves for osteons and interstitial matrix (maximum load 20 mN, loading rate 0.5 mN/s) for two dwell times: 0 s (a) and 120 s (b)
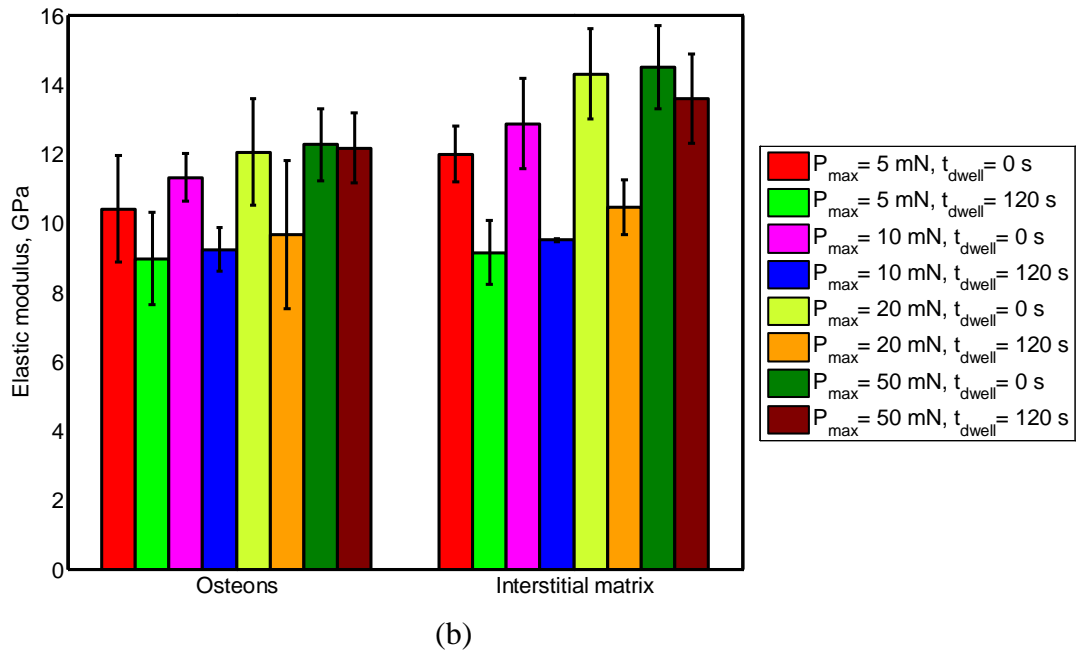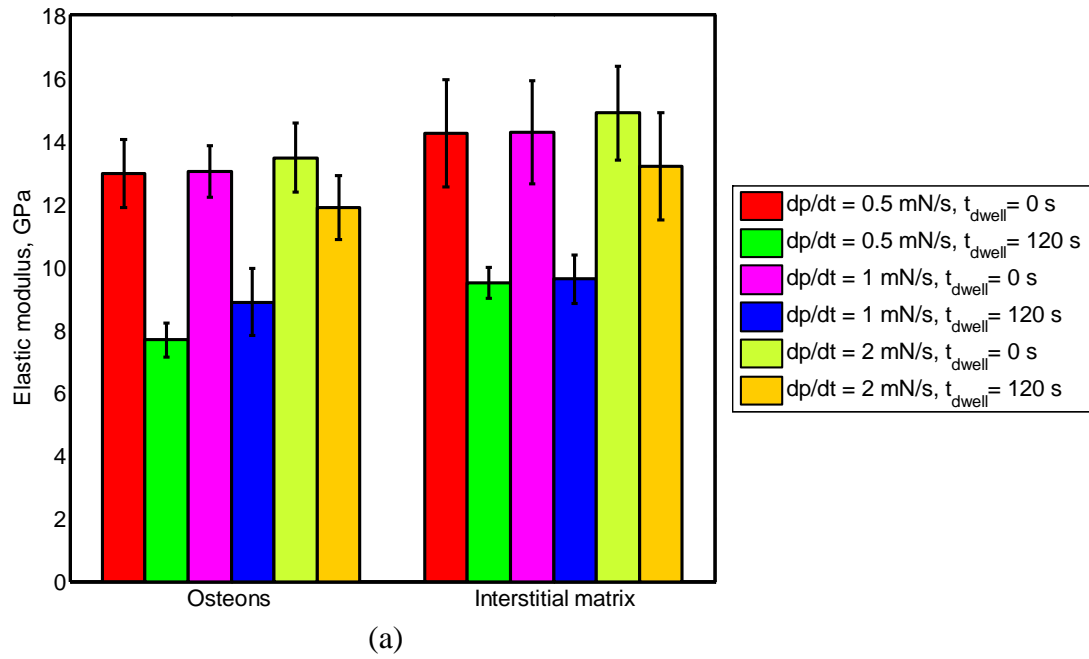
Figure 7: Elastic modulus for osteons and interstitial matrix: (a) effect of loading-unloading rate and dwell time at maximum load 10 mN; (b) effect of maximum applied load and dwell time at loading-unloading rate 0.5 mN/s
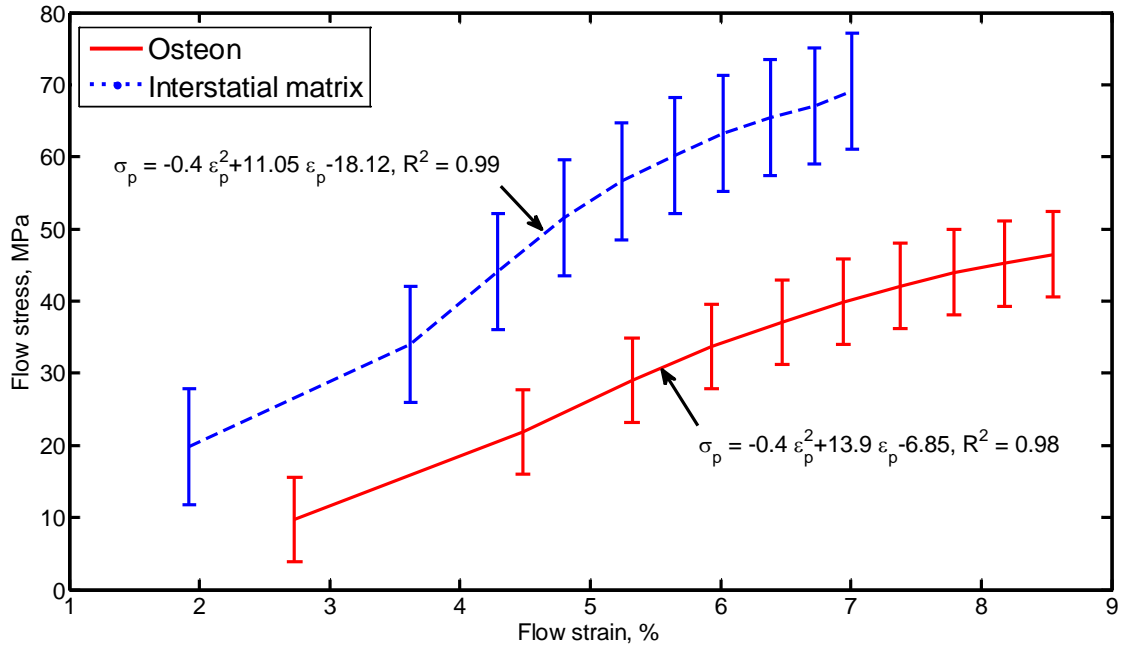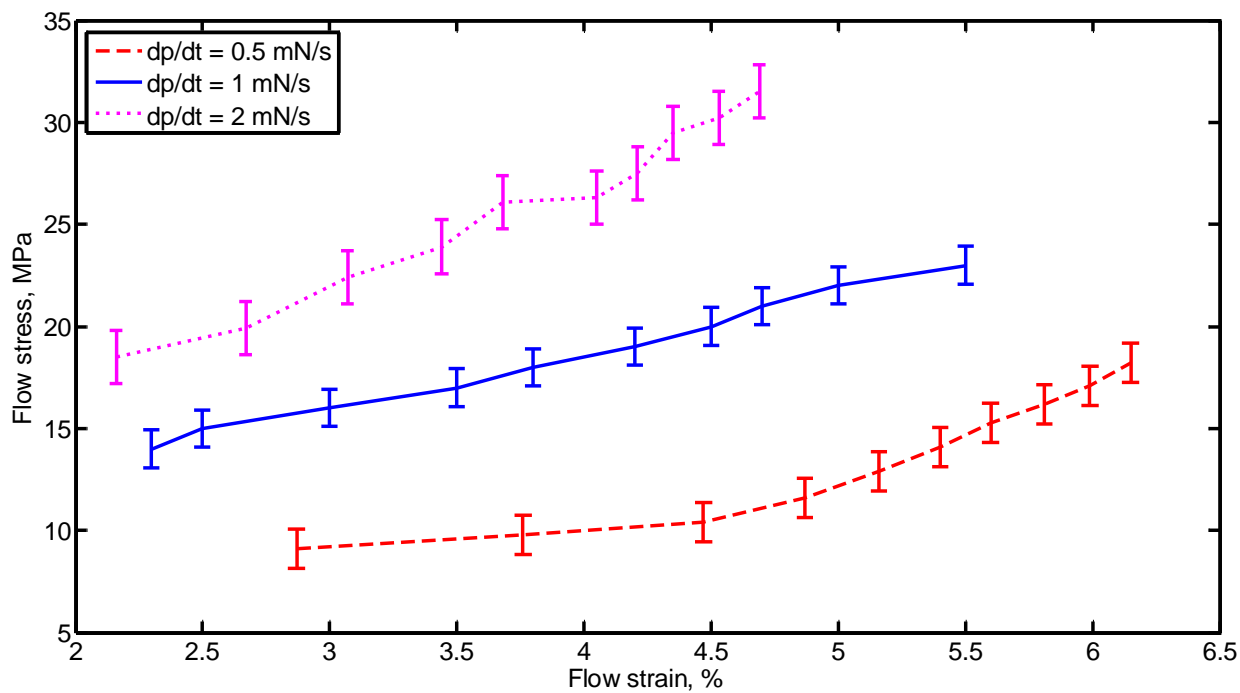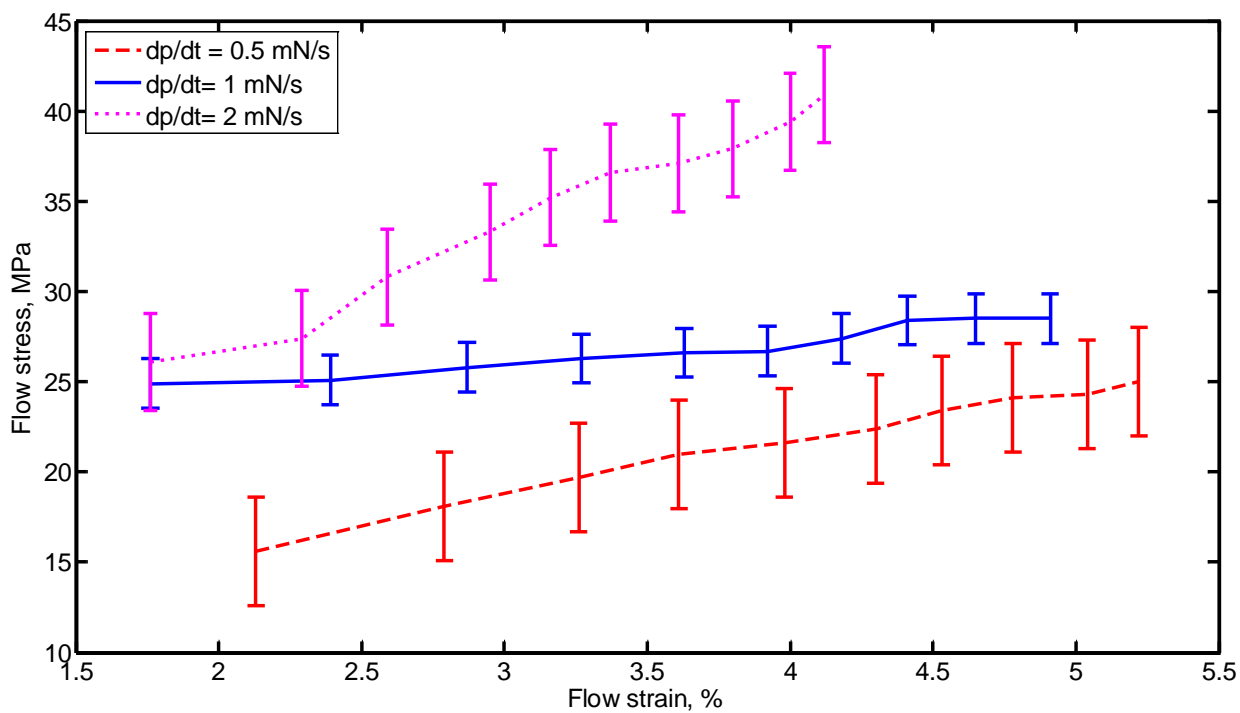
Figure 8: Flow stress-flow strain graphs for osteons and interstitial matrix (maximum load 50 mN; loading-unloading rate 0.5 mN/s; dwell time 120 s). Error bars show standard deviation
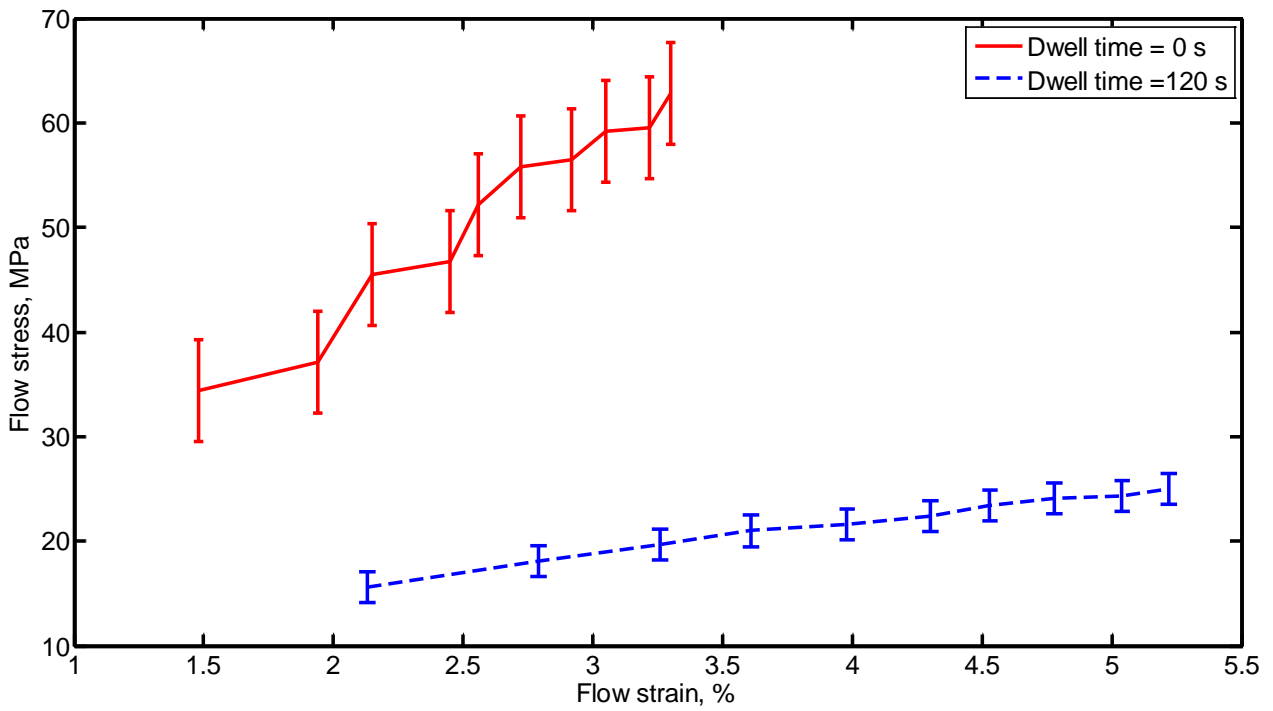
(a)

(b)
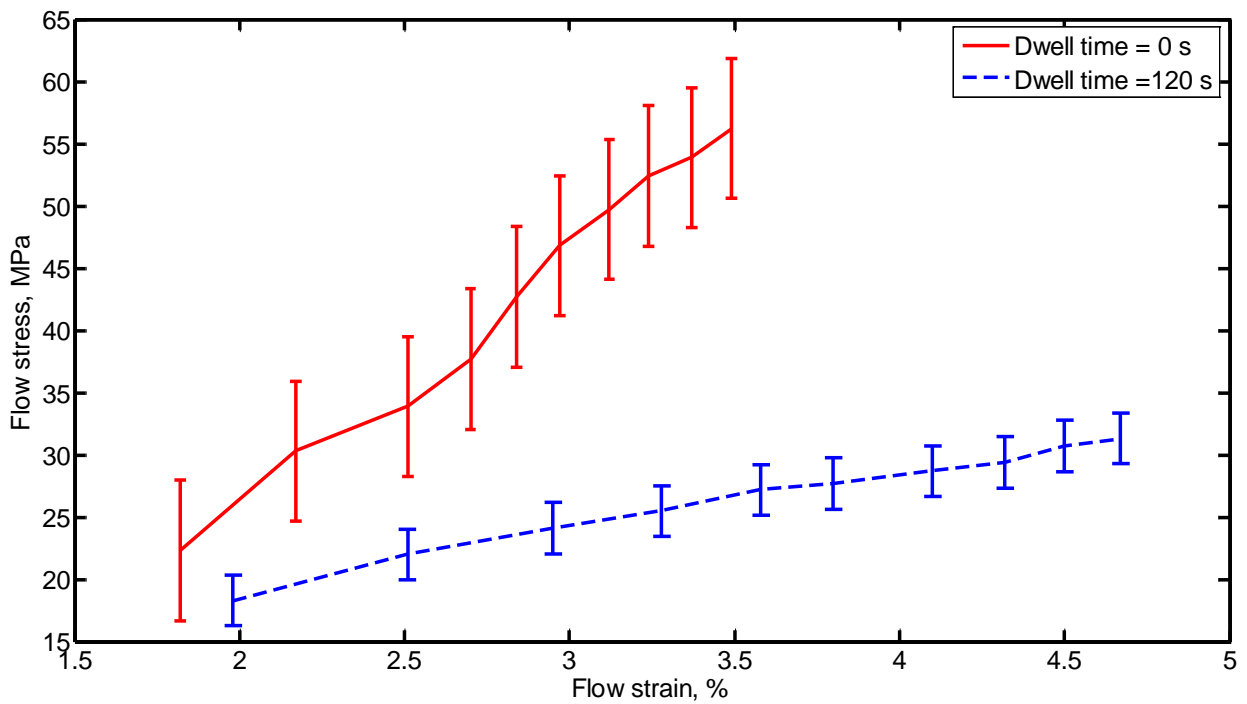
Figure 9: Effect of loading-unloading rate on flow stress-flow strain graphs (maximum load 10 mN; dwell time 120 s): (a) osteons; (b) interstitial matrix. Error bars show standard deviation

(a)

(b)

Figure 10: Effect of dwell time on flow stress-flow strain graphs (maximum load 10 mN; loading-unloading rate 0.5 mN/s): (a) osteons; (b) interstitial matrix. Error bars show standard deviation

Appendix

1. Nanoindentation

Nanoindentation has been widely used by the materials science community; for instance, it is employed for probing surface properties of thin films, small volumes, and microstructural features (Oliver and Pharr 1992). A schematic illustration of a nanoindentation load-displacement curve is shown in Fig. 4.

1.1.Theoretical Basis

The theoretical basis of nanoindentation method relies on solution of the problem of indentation of an elastic half-space with a rigid axis-symmetrical indenter derived by Sneddon (1965). The mathematical solution was adjusted by Oliver and Pharr (1992). Measurements of load-displacement curves from nanoindentation experiments are utilized to determine the contact stiffness, from which the indentation modulus can be calculated.

The relationship between elastic properties of a sample and contact stiffness is as follows:

$$S = \frac{dP}{dh} = \beta \frac{2}{\sqrt{\pi}} E_r \sqrt{A}, \qquad (1)$$

where P is the applied load, h is the indentation depth, A is the projected contact area of the indenter and function of depth h, and β is an empirical shape factor ($\beta = 1.034$ for a Berkovich indenter). To account for a non-rigid indenter used, a reduced modulus E_r is implemented and determined as follows:

$$\frac{1}{E_r} = \frac{(1 - v_s^2)}{E_s} + \frac{(1 - v_i^2)}{E_i}, \qquad (2)$$

where E_s and v_s are the elastic modulus and Poisson's ratio of the specimen, respectively, and E_i and v_i are the respective parameters of the indenter. In Eq. (2) the specimen is considered as an isotropic material, and the Poisson's ratio value has to be known. For a diamond indenter tip an elastic modulus is 1141 GPa and a Poisson's ratio is 0.07 (Oliver and Pharr 1992). The shape factor β=1 for a spherical diamond indenter, which was used in our study.

Hardness of the cortical bone tissue's constituents can be calculated as follows:

$$H = \frac{P_{max}}{A}, \qquad (3)$$

where P_{max} is the maximum indentation load and A is the corresponding projected area.

In general, nanoindentation reveals a wealth of information about the mechanics and mechanisms of thin films or small volumes of the studied material. This information includes levels of the elastic modulus, hardness, surface adhesion, creep, and stress relaxation behaviours. Moreover, it can also be used to obtain the flow stress-flow strain behaviour; the respective methodology is described elsewhere in (Zihiqiang and Zhang 2008).

1.2. Spherical-Indentation Theory

Sharp-tipped indenters don't allow a smooth transition between elastic and plastic behaviour of the material because they produce a constant strain impression (Oliver and Pharr 1992). On the other hand, spherical indenters provide a smooth transition and evaluation of the elastic-plastic behaviour of the material because an increasing contact stress is developed with the increasing indentation load. The model used to investigate the effects of geometry on local elastic deformation properties was first considered by Heinrich Hertz in 1882. In Hertizian contact, the circular contact area of two contacting spheres is related to the elastic deformation properties of the materials. The radius of that area predicted by Hertizian analysis is given as follows (Micro Materials Ltd 2004):

$$a = \left(\frac{3PR_s}{4E_r}\right)^{1/3}, \qquad\qquad (4)$$

where P is the applied load, R_s is the radius of the sphere, and E_r is the reduced modulus given in Eq. 2.

For static Hertizian contact, the maximum shear stress is situated at a distance of approx. half the contact radius measured from the point of contact. On the other hand, yielding first takes place below the surface when

$$P_m = 1.1\, Y, \q\qquad\qquad (5)$$

where P_m is the mean pressure and Y is the yield stress. The contact remains elastic if the mean pressure is less than this value.

An indentation process may produce one of three possible types of deformation: (i) reversible, elastic; (ii) permanent, plastic; or (iii) both elastic and plastic. The ratio between the actual strain and the yield strain of the material determines its behaviour during indentation process. The elastic behaviour can be obtained for low ratios (less than 2), and the behaviour can be considered purely plastic for high ratios (higher than 50). The value of the actual strain is given by $\tan\emptyset$, where $\emptyset$ is the angle between the indenter and sample surfaces; it is obvious that a spherical and pyramid indenter will behave differently. In the case of a Vickers pyramid, for instance, $\emptyset$ is constant and the strain is therefore constant (8%), regardless of depth. On the other hand, for a spherical indenter, $\emptyset$ and, therefore, strain increases with indentation depth. Consequently, a series of spherical indentations with an increasing maximum load can produce results ranging from purely elastic to elastic-plastic deformation in addition to stress-strain curves (Micro Materials Ltd 2004).

By performing multiple loading-unloading cycles with increasing maximum loads at a single point using a spherical indenter with a known radius, the contact area, hardness, elastic modulus as well as stress and strain can be calculated.

1.3. Spherical Indentation Analysis Procedure

For a given indentation experiment consisting of n indentation cycles, the related total penetration depth is h_t at a load P_t and a partially recovered depth h_s at a reduced load of P_s. The depth h_r of the residual impression relative to the specimen original surface for a fully unloaded indenter can be calculated as follows (Micro Materials Ltd 2004):

$$h_r = \frac{rh_s - h_t}{r - 1}, \qquad\qquad (6)$$

where

$$r = \left(\frac{P_t}{P_s}\right)^{\frac{2}{3}}. \tag{7}$$

The elastic component h_e and the plastic component h_p of the indentation at each cycle can be calculated as follows:

$$h_e = h_t - h_r, \tag{8}$$

$$h_p = \frac{h_t + h_r}{2}. \tag{9}$$

The contact circle radius a in the original surface plane at each indentation cycle can be calculated as follows:

$$a = \sqrt{\left(2R_s h_p - h_p^2\right)}, \tag{10}$$

Hardness H, reduced modulus E_r, flow stress σ_r and corresponding flow strain ε_r at each indentation cycle i can be calculated as follows (Micro Materials Ltd 2004):

$$H_i = \frac{P_{t_i}}{\pi a_i^2}, \tag{11}$$

$$E_{r_i} = \frac{3}{4}\frac{P_{t_i}}{a_i h_{e_i}}, \tag{12}$$

$$\sigma_{r_i} = \frac{H_i}{3}, \tag{13}$$

$$\varepsilon_{r_i} = 0.2\,\frac{a_i}{R}, \tag{14}$$

where $i = 1$ to N.

To account for the possibility of piling-up or sinking-in around the spherical indenter contact, the true contact circle radius a_r is related to a determined above by the following function:

$$a_r = ca. \tag{15}$$

The value of the constant c can be determined as follows: first from plotting a $P_{t_i} - a_i$ diagram in double logarithmic coordinates, the Meyer's index $(2 + 1/n)$ is calculated as the slope of the diagram, and then c can be obtained as

$$c^2 = \frac{5}{2}\frac{2n-1}{4n+1}. \tag{16}$$

Then, correction factors $1/c^2$ and $1/c$ should be applied to hardness H and the reduced modulus E_r, respectively.